LUT University
LUT School of Energy Systems
LUT Mechanical Engineering
BK10A0402 Kandidaatintyö

THE EFFECT OF MANUFACTURING PARAMETERS ON THE MECHANICAL PROPERTIES OF L-PBF PRODUCED 420 STAINLESS STEEL

VALMISTUSPARAMETRIEN VAIKUTUS LASER-JAUHEPETISULATETUN RUOSTUMATTOMAN TERÄKSEN 420 MEKAANISIIN OMINAISUUKSIIN

Lappeenranta 22.04.2021
Lari Rajala
Examiner Professor Heidi Piili, D.Sc. (Tech.)
Supervisors Professor Heidi Piili, D.Sc. (Tech.)
Postdoctoral research scientist Mohsen Amraei, Ph.D.

TIIVISTELMÄ

LUT-yliopisto
LUT Energiajärjestelmät
LUT Kone

Lari Rajala

Valmistusparametrien vaikutus laser-jauhepetisulatetun ruostumattoman teräksen 420 mekaanisiin ominaisuuksiin

Kandidaatintyö

2021

28 sivua, 10 kuvaa, 5 taulukkoa ja 2 liitettä

Tarkastaja: Professori Heidi Piili, TkT

Ohjaaja: Professori Heidi Piili, TkT
Tutkijatohtori Mohsen Amraei, FT

Hakusanat: laser-jauhepetisulatus, ruostumaton teräs, lisäävä valmistus, valmistusparametri, AISI 420, X20Cr13

Tämän kandidaatintyön tarkoituksena oli selvittää valmistusparametrien vaikutus laser-jauhepetisulatetun (L-PBF, eng. laser powder bed fusion) ruostumattoman teräksen 420 mekaanisiin ominaisuuksiin. Työ suoritettiin kirjallisuuskatsauksena ja siinä selvitettiin perinteisillä menetelmillä valmistetun ruostumattoman teräksen 420 mekaaniset ominaisuudet, L-PBF:n valmistusparametrit sekä aiemmissa tutkimuksissa havaitut L-PBF valmistetun ruostumattoman teräksen 420 mekaaniset ominaisuudet.

Ruostumaton teräs 420 on martensiittinen ruostumaton teräs, joka on lujaa sekä korroosionkestävää. Valmistusparametreiksi todettiin lasersäteen teho P, skannausnopeus v, kerrospaksuus t ja skannausetäisyys h, sekä näistä laskettava tilavuudellinen energiatiheys E_v.

Aiemmista tutkimuksista havaittiin, että L-PBF:llä voidaan valmistaa ruostumatonta terästä 420, jonka mekaaniset ominaisuudet vastaavat perinteisillä menetelmillä valmistettua ruostumatonta terästä 420. Tilavuudellisen energiatiheyden E_v kasvattaminen parantaa L-PBF-tulostetun ruostumattoman teräksen 420 lujuusominaisuuksia, mutta sillä ei näytä olevan vaikutusta kovuuteen. Muut parametrit ovat myöskin tärkeitä, koska muutoin voi esiintyä valmistusvirheitä kuten avaimenreikähuokoisuutta tai puutteellisen yhteensulamisen aiheuttamaa huokoisuutta.

ABSTRACT

LUT University
LUT School of Energy Systems
LUT Mechanical Engineering

Lari Rajala

The effect of manufacturing parameters on the mechanical properties of L-PBF produced 420 stainless steel

Bachelor's thesis

2021

28 pages, 10 figures, 5 tables, and 2 appendices

Examiner: Professor Heidi Piili, D.Sc. (Tech.)

Supervisor: Professor Heidi Piili, D.Sc. (Tech.)
Postdoctoral research scientist Mohsen Amraei, Ph.D.

Keywords: L-PBF, stainless steel, additive manufacturing, manufacturing parameter, AISI 420, X20Cr13

The aim of this bachelor's thesis is to find how manufacturing parameters affect the mechanical properties of laser powder bed fusion (L-PBF) manufactured 420 stainless steel. The thesis is conducted as a literature review. In the thesis, the mechanical properties of wrought 420 stainless steel, the manufacturing parameters in L-PBF, and the mechanical properties of L-PBF manufactured 420 stainless steel in literature are discussed.

420 stainless steel has a martensitic microstructure, thus, it comprises good tensile strength and corrosion properties. Laser power P, scan speed v, layer thickness t, and hatch distance h are chosen as manufacturing parameters along with their combination volumetric energy density E_v.

It was found that with L-PBF it is possible to produce 420 stainless steel that has comparable mechanical properties to wrought 420 stainless steel. By increasing the E_v, the tensile strength of L-PBF produced 420 increases too, however, it did not seem to have significant effect on the hardness values. The other parameters were also important as their improper selection may lead to defects such as keyhole porosity or lack-of-fusion.

TABLE OF CONTENTS

LIST OF SYMBOLS AND ABBREVIATIONS

R_m	Ultimate tensile strength [MPa]
$R_{0,2}$	Yield strength or proof stress at 0,2% elongation [MPa]
P	Laser power [W]
v	Laser scan speed [mm/s]
t	Layer thickness [mm]
h	Hatch distance [mm]
E_v	Volumetric energy density [J/mm^3]
ε	Elongation [%]
ρ	Density [kg/m^3]

AM	Additive manufacturing
L-PBF	Laser powder bed fusion

1 INTRODUCTION

Additive manufacturing (AM) refers to the manufacturing method in which material is added to the desired locations to form a structure layer-by-layer. The parts are typically designed using a CAD software, creating a 3D model that is then sliced to build the layers as a STL file. The STL file is then imported to the AM machine for building. What sets AM apart from conventional manufacturing processes is that it does not need critical thinking in the order of manufacturing, or what tooling and processes are required to form a complete part. (Gibson et al. 2021, p. 1-5)

Typical AM processes for metal include laser powder bed fusion (L-PBF) and binder jetting. Laser-based powder bed fusion (L-PBF) is an AM process where powder material is melted together via a laser beam. The laser beam scans a powder bed layer-by-layer to produce a dense part. This thesis will focus on L-PBF. As an example, binder jetting is another powder bed process, where the powder is bound together with a binder that is jetted on the powder bed i.e., the material is not melted together. As such post-processing is required where the binder is removed from the finished part, the material is solid state sintered to keep the structure intact, and infiltration may be used to improve density and strength. (Kumar 2020, p. 44, 88.)

There is little to none up to date information about L-PBF manufacturing of 420 stainless steel. Therefore, updated information about 420 grade stainless steel is needed. Especially when it comes to L-PBF process and the effect of its process parameters on the properties of 420 stainless steel. The process parameters in AM have an effect on the microstructure of the material that in turn affect the mechanical properties of the material. As such, it is crucial to know the optimal parameters to obtain the desired properties for different applications.

Hence, the research questions of this thesis are as following:

- What is the most important parameter when manufacturing 420 stainless steel?
- How the effects of different parameters to 420 stainless steel have been studied?
- What effects different parameters have on the mechanical properties of manufactured 420 stainless steel?

This thesis conducts as a literature review with focus on L-PBF produced 420 stainless steel. Primarily, Primo and Scopus (at LUT Library) are used to search for the available data in the literature. 420 stainless steel manufactured with L-PBF is studied by looking at previous studies, listing the used manufacturing parameters, and the achieved mechanical properties of the material produced with L-PBF. Mechanical properties of wrought 420 stainless steel is shown, to better evaluate the mechanical properties achieved with L-PBF, as a reference. Also, manufacturing parameters are discussed along the general defects that can be attributed to them.

Results of this thesis will be used around the research activities of LUT University's Research Group of Laser Materials Processing and AM. It also gives valuable insight for the companies that are wishing to utilize additively manufacture 420 stainless steel in their production line. Also, if this thesis finds that there is not enough information on the subject, or there are clear gaps, it will give a reason to study it further.

2 420 STAINLESS STEEL

AISI 420 is a martensitic stainless steel grade. As a martensitic steel it has great strength and hardness, and as being a stainless steel, it offers corrosion resistance (Nath et al. 2019; Saeidi et al. 2019). Typical areas where it is utilized include dental and surgical instruments, cutlery, glass and plastics processing tools among others (Brnic et al. 2011).

This steel grade is comparable to X20Cr13, X30Cr13, X39Cr13, X46Cr13 and X52Cr13 of the EN standard (SFS-EN 10088-1 2014). Only X20Cr13 of the EN standard is discussed in this thesis alongside AISI 420. Table 1 shows the chemical composition of X20Cr13 and AISI 420, and Table 2 presents some of their properties from various sources.

Table 1. The chemical composition of AISI 420 and X20Cr13.

Element	Mass percent [%]	
	AISI 420 (Davis 1998)	X20Cr13 (SFS-EN 10088-3 2014)
Carbon, C	0.15 (min)	0.16-0.25
Chromium, Cr	12.00-14.00	12.00-14.00
Silicon, Si	1.00	1.00
Manganese, Mn	1.00	1.50
Phosphorus, P	0.04	0.04
Sulphur, S	0.03	0.03

Table 2. The properties of AISI 420 and X20Cr13.

	AISI 420 (Davis 1998)	AISI 420 Annealed/Hardened (Coleman et al. 2013)		Outokumpu 4021 (Outokumpu Stainless 2013)	X20Cr13 Quenched & tempered (SFS-EN 10088-3 2014)
Density, ρ [kg/m^3]	~8	7.74		7.7	7.7
Ultimate tensile strength, R_m [MPa]	1720	586	1586	650	800 - 950
Yield strength at 0,2 % elongation, $R_{0,2}$ [MPa]	1480	276	1344	500	600
Elongation, ε [%]	8	25	8	20	12
Hardness	52 HRC	88 HRB	55 HRC	-	-

As it can be seen from Table 2, there are considerable variations on the reported mechanical properties of 420 stainless steel. The difference might be due to different heating/cooling cycles during the manufacturing. Tensile testing by Brnic et al. (2011) also showed $R_{0,2}$ to be 650 MPa and R_m to be 840 MPa at room temperature.

3 MANUFACTURING PARAMETERS

The optimization of parameters in L-PBF is valuable in order to produce parts that are dense with desired quality, as well as material properties. The most effective process parameters are considered to be laser power *P*, scanning speed *v*, layer thickness *t*, hatch distance *h*, and scanning pattern (Oliveira, LaLonde & Ma 2020, p. 1). Figure 1 shows those parameters schematically. All the forementioned parameters, but scanning pattern, which is considered to be a manufacturing parameter, will be discussed further.

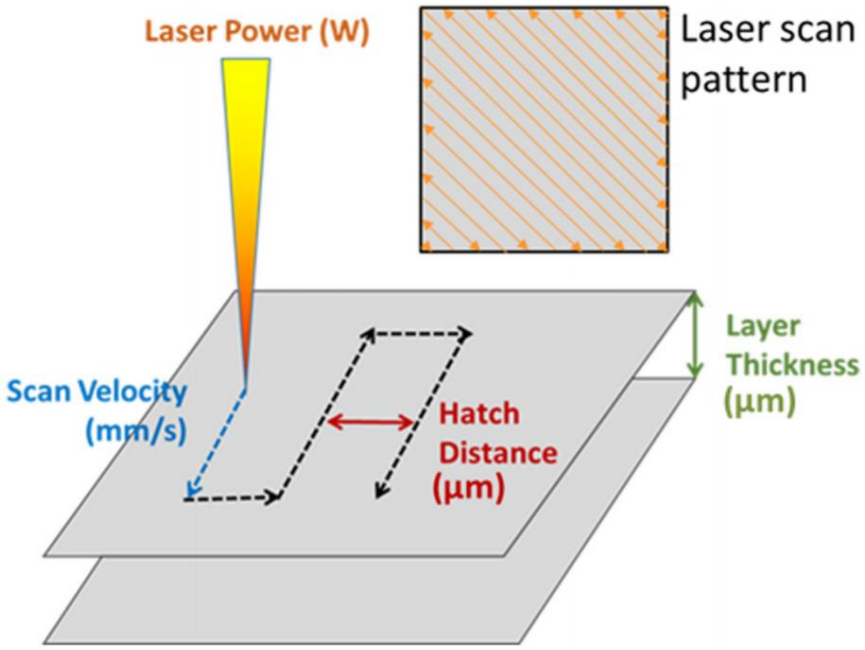

Figure 1. A schematic illustration of the most common process parameters in L-PBF process. (Oliveira et al. 2020, p. 2)

The laser material interaction in L-PBF sees the energy of the laser beam being absorbed by the powder, and as a result the powder melts, forming a melt pool. In the conduction mode, the formed melt pool has a depth that reaches beyond the powder layer, into the solid material to fuse them completely. There is a cavity formed on the boundary of the melt pool and powder bed where the laser heats the front of the cavity. (Saunders 2017.)

Scan speed *v* is the velocity at which the laser beam passes on the powder bed. Optimal scanning speed is needed to be determined, as otherwise, build defects or long production times are expectable. Its value is dependent also on the laser power *P* regarding the defects as illustrated in **Error! Reference source not found.**.

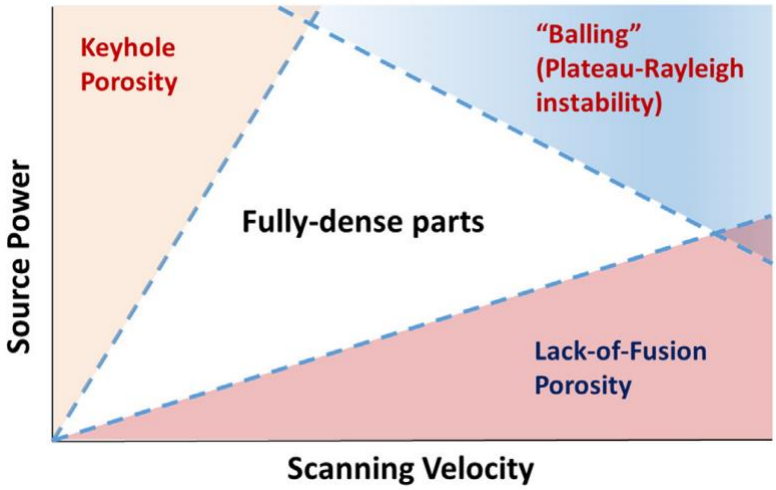

Figure 2. The effects of laser power in relation to scanning speed. (Oliveira et al. 2020, p. 4)

It can be seen from figure 2 that at a low scanning speed *v* and a high laser power *P* will lead to keyhole porosity, where the laser interaction transfers from conduction mode to keyhole mode. (Oliveira et al. 2020, p. 4.) When the mode transfers to keyhole, the melt pool reaches the previous layer over the needed depth due to the increased energy that enlarges the depth of cavity. The rise in energy increases turbulence in melt pool, and the formation of spatters. The pores that are created in keyhole mode are caused by the collapse of the melt pool on to the keyhole cavity due to the melt pool becoming unstable. (Saunders 2017.)

An opposite to keyhole porosity is the lack-of-fusion that is caused by high scanning speed compared to laser power, and as a result, the laser is unable to form a uniform melt pool (Oliveira et al. 2020, p. 4). With the lack-of-fusion, the powder layer is not being fully melted. As the result, porosity is formed by the un-melted powder being trapped within solidified material (Saunders 2017.).

Hatch distance *h* is the distance between two adjacent passes as shown in Figure 1. It is essential to have an overlap in melt pools to produce fully dense parts, otherwise, there will

be a gap between the melt pools that will lead to porosity. Layer thickness *t* is the height at which the 3D model is sliced to layers and the height at which the actual layers are built during the L-PBF process. Increase of layer thickness *t* will also cause higher production speed, although it will require higher laser power to create a melt pool that will achieve full fusion and the precision of produced parts will decrease. (Kumar 2020, p. 48–49.)

By combining the four previously mentioned parameters, volumetric energy density E_v can be calculated, as equation 1 shows (Nath et al. 2019, p. 740; Kumar 2020, p. 49):

$$E_v = \frac{P}{h\ v\ t} \tag{1}$$

where *h* is hatch distance (mm), *v* is scanning speed (mm/s), *t* is layer thickness (mm) and *P* is laser power (W). E_v is a widely used parameter in literature (Nath et al. 2019; Saeidi et al. 2019; Tian, Chada & Aranas 2021; Shi et al. 2020; Shen et al. 2020). The volumetric energy density affects the properties and microstructure of the manufactured product. However, it consists of different parameters, which means that with the same value of energy density but with different values on the influencing parameters, a diverse range of end properties can be achieved.

4 REVIEW OF STUDIES ON L-PBF PRODUCED 420 STAINLESS STEEL

There have been various studies on the mechanical properties of 420 stainless steel fabricated by L-PBF (Nath et al. 2019; Nath et al. 2020; Tian et al. 2021; Saeidi et al. 2019; Shi et al. 2020; Shen et al. 2020). In this chapter the reported mechanical properties of 420 stainless steel produced with L-PBF and the manufacturing parameters used are reported.

4.1 Used equipment and powders

The equipment and powders that are used in the literature are reported in this section. The parameters used in different studies are listed in Table 3, and chemical compositions of the powders in Table 4.

Nath et al. (2019) fabricated 420 stainless steel from nitrogen gas atomized pre-alloyed powder provided by Sandvik Osprey. The chemical composition of the powder was reported to be comparable to wrought 420. Their studied specimens were produced using Concept Laser Mlab cusing R machine with an Yb-fiber laser. The specimens were produced in argon atmosphere. The specimens were fabricated with E_v of 63 J/mm^3, using following parameters:

- Laser power P = 90 W
- Scan speed v = 600 mm/s
- Layer thickness t = 20 μm
- Hatch distance h = 120 μm. (Nath et al. 2019, p. 739.)

Nath et al. (2020) examined the effect of layer thickness t on L-PBF fabricated 420 stainless steel. The used powder and equipment were the same as in study by Nath et al. (2019) . P, h and v were kept as constant with the values being 90 W, 120 μm and 600 mm/s, respectively. Layer thicknesses t of 10, 20 and 30 μm were used accordingly. (Nath et al. 2020, p. 1198.)

Tian et al. (2021) fabricated 420 stainless steel with E_v in the range of 75 to 85 J/mm^3. The parts were produced using an EOS M290 machine in argon atmosphere. The provider of the powder was not disclosed in their study. The parameters were listed as varying with P being

240-280 W, *v* being 1000-1200 mm/s, *h* being 80-120 μm, and *t* being 30 μm. Using the average parameter values E_v can be calculated to be 80 J/mm^3. (Tian et al. 2021, p. 5.)

Saeidi et al. (2019) fabricated 420 stainless steel using EOS M270 machine with an Yb-fiber laser. The atmosphere at which the parts were produced was unspecified. The powder used was gas atomized provided by Sandvik Osprey. The parts were produced by *P* of 195 W, *v* of 700 mm/s, *t* of 20 μm, and *h* of 100 μm. E_v was calculated to be 139 J/mm^3. (Saeidi et al. 2019, p. 2.)

Shi et al. (2020) used Ranishaw AM250 machine with a pulse laser to fabricate 420 stainless steel. The used parameter values were 200 W, 115 μm, 30 μm and 680 mm/s for *P*, *h*, *t* and *v*, respectively, with E_v totalling to 85 J/mm^3. The build atmosphere along with the source of used powder were unspecified. (Shi et al. 2020, p. 1467–1468.)

Shen et al. (2020) used Sandvik Osprey's 420 stainless steel powder to fabricate the test specimens. The samples were built with OPM259L L-PBF machine with a Yb-fiber laser. The *v* of 700 mm/s, *t* of 50 μm and *h* of 200 μm were used in this study. The initial *P* was 420 W for the first three layers, for the powder to better fuse with the baseplate, after which *P* was reduced to 400 W with the E_v values being 60 J/mm^3 and 57 J/mm^3, respectively. The baseplate was preheated to 180 °C and the building atmosphere was not disclosed. (Shen et al. 2020, p. 3.)

Table 3. Used manufacturing parameters in literature.

Article	Laser power, P [W]	Scan speed, v [mm/s]	Layer thickness, t [μm]	Hatch distance, h [μm]	Volumetric energy density, E_v [J/mm^3]	Build atmosphere
(Nath et al. 2019)	90	600	20	120	63	Argon
(Nath et al. 2020)	90	600	10	120	125	Argon
			20		63	
			30		42	
(Tian et al. 2021)	260	1100	30	100	80	Argon
(Saeidi et al. 2019)	195	700	20	100	139	-
(Shi et al. 2020)	200	700	30	115	85	-
(Shen et al. 2020)	400	700	50	200	57	-

Table 4. The chemical compositions of the powders.

Article	Mass percent [%]					
	C	Cr	Si	Mn	P	S
(Nath et al. 2019)	0.30	12.80	0.79	0.72	0.012	0.008
(Nath et al. 2020)	0.30	12.80	-	0.78	-	-
(Tian et al. 2021)	0.15	13.00	1.00	1.00	0.070 (combined)	
(Saeidi et al. 2019)	0.30	13.00	0.80	0.80	-	-
(Shi et al. 2020)	0.23	12.55	0.94	1.05	0.013	0.009
(Shen et al. 2020)	0.35	13.00	1.00	1.00	-	-

4.2 Heat treatments

Heat treatment as a post-processing method can have significant effect on the microstructure, and the mechanical properties of AM parts (Gibson et al. 2021, p. 478). Hence, the available treatments in the literature and their impact on the L-PBF parts made of 420 stainless steel are discussed in this section. Out of the studied articles all except Shen et al. (2020) used heat treatments. The first two studies employed the same heat treatment after L-PBF process. In their studies, the parts were heated for 2 hours at 315 °C after which they were air cooled. (Nath et al. 2019, p. 739; Nath et al. 2020, p. 1198.)

Tian et al. (2021) first heated the parts at 1043 °C for 1h after which they were gas quenched in nitrogen with 5 to 6 bar pressure. Then the parts were tempered for 3 hours at 182 °C two times, where the parts were air cooled in between. A vacuum environment was employed though out the process. (Tian et al. 2021, p. 6.)

Saeidi et al. (2019) tempered the parts in a tube furnace. The parts were first heated up with the rate of 300 °C/h and held at 400 °C for 15 min. The parts were left to cool inside the

furnace at the end. An argon atmosphere was maintained throughout the process. (Saeidi et al. 2019, p. 2.)

Shi et al. (2020) austenitized the manufactured parts in a vacuum furnace at 1000 °C temperature for 40 minutes after which they were gas quenched. After that, the parts were tempered at 560 °C for 3 hours with a gas cooling afterwards. (Shi et al. 2020, p. 1468.)

4.3 Mechanical properties

The testing methods used in various studies are described in this section. The mechanical properties achieved are listed in Appendix I. If hardness was listed as other than HRC, the original value is shown followed by conversion to HRC according to conversion table by Thompson (1999).

The first two studies (Nath et al. 2019; Nath et al. 2020) did the tensile testing according to ASTM E8 with gauge dimensions of 35 x 6.2 x 3 mm and with the total length of the test pieces being 75 mm. Four samples were used per material condition. Tensile testing was conducted with MTS Exceed machine with a 100 kN load cell, at the strain rate of 0.001 s^{-1}. Hardness was measured from the scan surface with a 150 kg load with a Rockwell C scale. Four test pieces were used to determine the hardness with 10 measurements per test pieces. (Nath et al. 2019, p. 739; Nath et al. 2020, p. 1199.)

Tian et al. (2021) used a Instron 1332 with 200 kN load cell to carry out the tensile tests. Test pieces had a length of 86 mm and a diameter of 14 mm. Two batches were used with the first one's lengths being parallel to the build direction, and the second's being parallel to transverse direction. Five tests were conducted per each condition. Charpy impact toughness tests were conducted on standard size 55 x 10 x 10 mm parts. Tensile tests were conducted according to ASTM E8 and Charpy tests according to ASTM E23. Hardness was not measured in this study (Tian et al. 2021, p. 6.)

Saeidi et al. (2019) used a gauge length of 25 mm with dog-bone-shaped test samples. The tensile test machine was Tiratest 2000 with the crosshead speed of 0.5 mm/min. Hence the strain rate of the tensile testing was 0.00033 s^{-1}. Hardness testing was conducted with

Zwick/Roell ZHV indenter using a load of 1 kg, and 10 s dwell time. Reported hardness values were an average of ten indents. (Saeidi et al. 2019, p. 2.)

Shi et al. (2020) used specimens with gauge dimension of 28 x 5 x 2 mm for tensile test samples that were in line with the Chinese testing standard GB/T228. Properties were examined in both longitudinal and transverse directions. Total of three measurement were taken per condition. Crosshead speed of 2 mm/min was used during tensile testing. Hardness values were measured with 62.5 kg load and a 2.5 mm diameter indenter. Six indents were made on each sample with a total of three samples per condition. (Shi et al. 2020, p. 1468.)

Shen at al. (2020) conducted the tensile tests with MTS 810. Three types of test samples were built with build direction being along the thickness, width, and length of the test pieces, respectively. The gauge dimensions were 32 x 6 x 3 mm with the crosshead speed of 0.5 mm/min until a strain of 1 % was reached. Afterwards, the test speed was increased to 2 mm/min. Hardness was determined with AR-10 tester in HRC with a load of 150 N. A total of ten indents per sample were made. (Shen et al. 2020, p. 4–5.)

Figures 33 to 5 show the correlation between R_m, $R_{0,2}$, and hardness as a function of E_v, respectively. Other graphs are included in Appendix II.

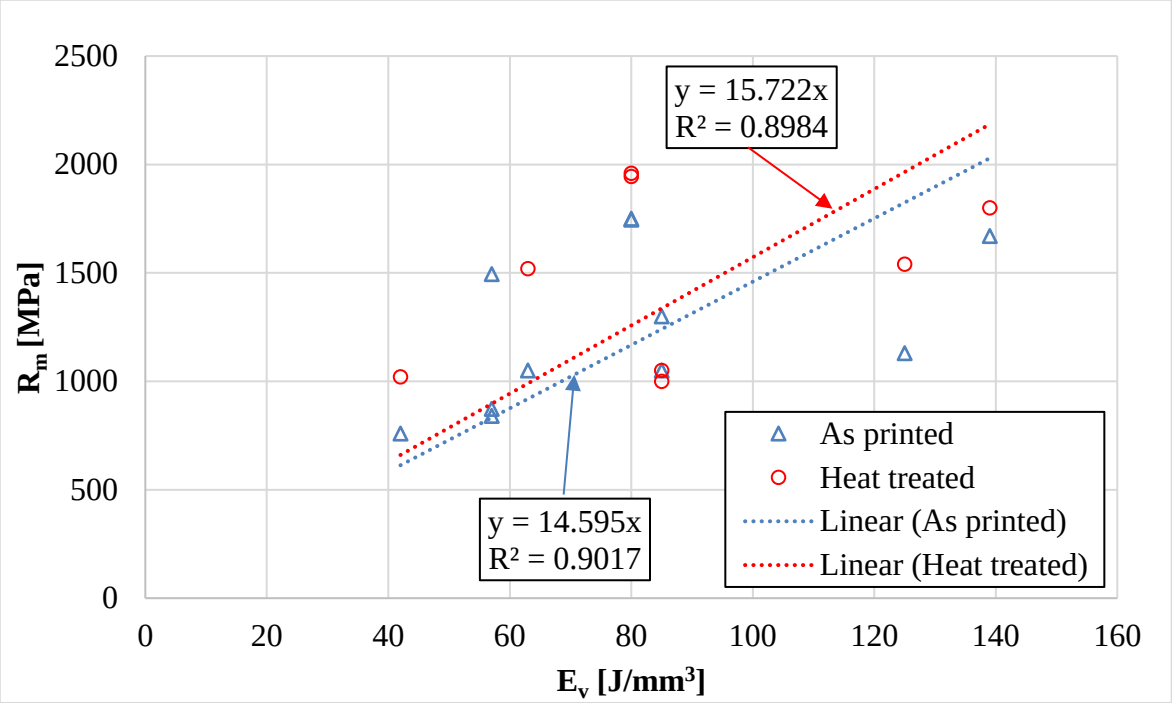

Figure 3. The correlation between R_m as a function of E_v.

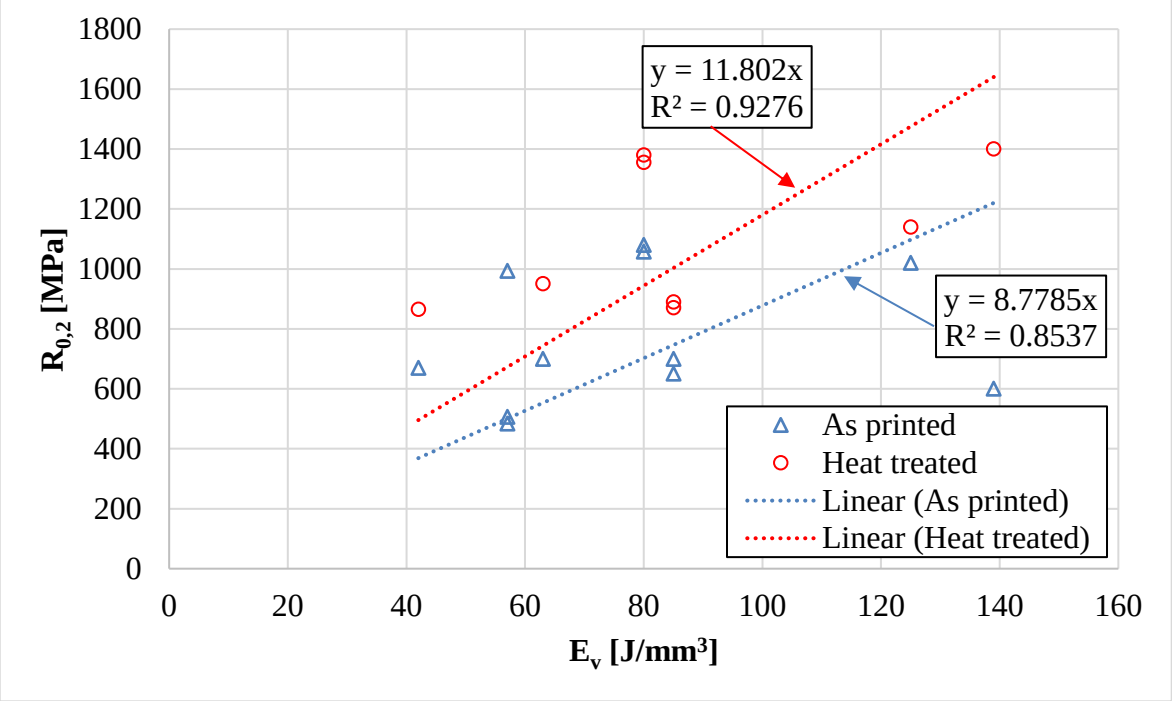

Figure 4. The correlation between $R_{0,2}$ as a function of E_v.

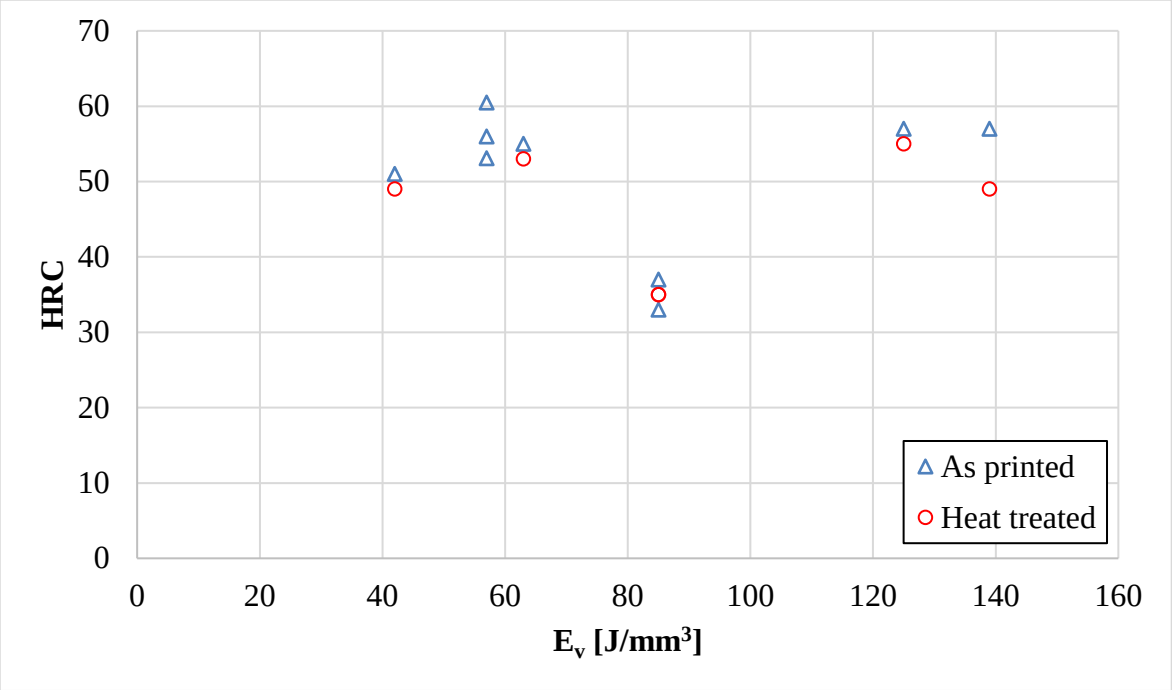

Figure 5. The correlation between hardness as a function of E_v.

All articles except Tian et al. (2021) reported the relative density of their manufactured specimens. The relative density compared to wrought 420 stainless steel was measured by Archimedes method and the values are listed in Table 5. In Figure 6 the correlation between relative density as a function of E_v is shown.

Table 5. Relative densities of the manufactured parts.

Article	Relative density (%)	Notes
(Nath et al. 2019)	99,2	-
(Nath et al. 2020)	99,6	t = 10 µm
	95,1	t = 30 µm
(Saeidi et al. 2019)	99,8	-
(Shi et al. 2020)	99,73	-
(Shen et al. 2020)	96	Built along thickness of part
	93	Built along width of part
	92	Built along length of part

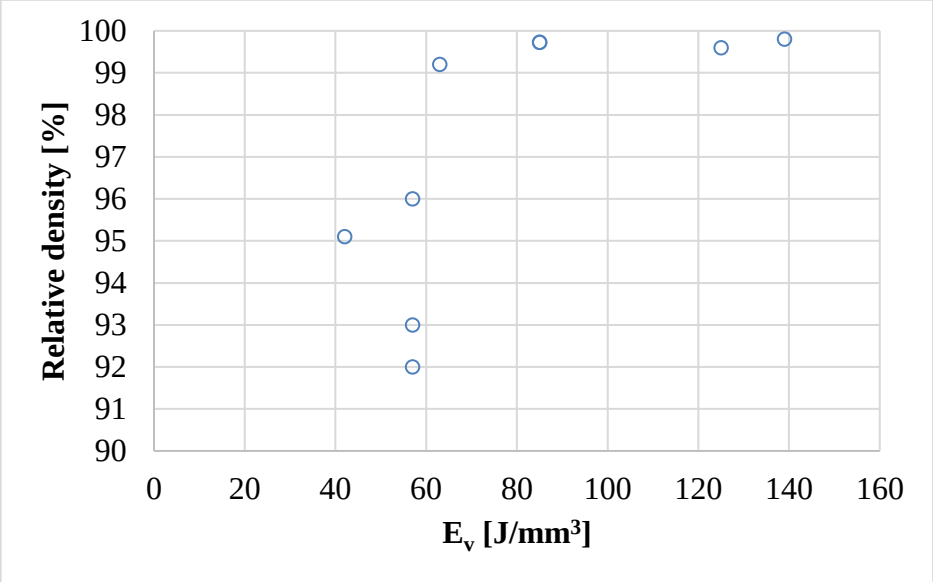

Figure 6. The correlation between relative density as a function of E_v.

4.4 Microstructure of the manufactured specimens

In this section the key outcomes from the microstructural analysis of the studied articles are presented. The microstructure of 420 stainless steel consists of austenite and martensite phases. Martensite appeared in laths or needles as shown in Figure 7 and Figure 8. In these figures martensite is appearing in darker and austenite in lighter colour (Nath et al. 2019). The increase of martensite content can be observed after heat treatment. Similar observation was reported by Tian et al. (2021) and Shi et al. (2020). In the build direction, the martensite laths were scattered irregularly whereas in the scan direction a pattern was observed with the laths being in the melt pool boundaries which can be seen in Figure 8.

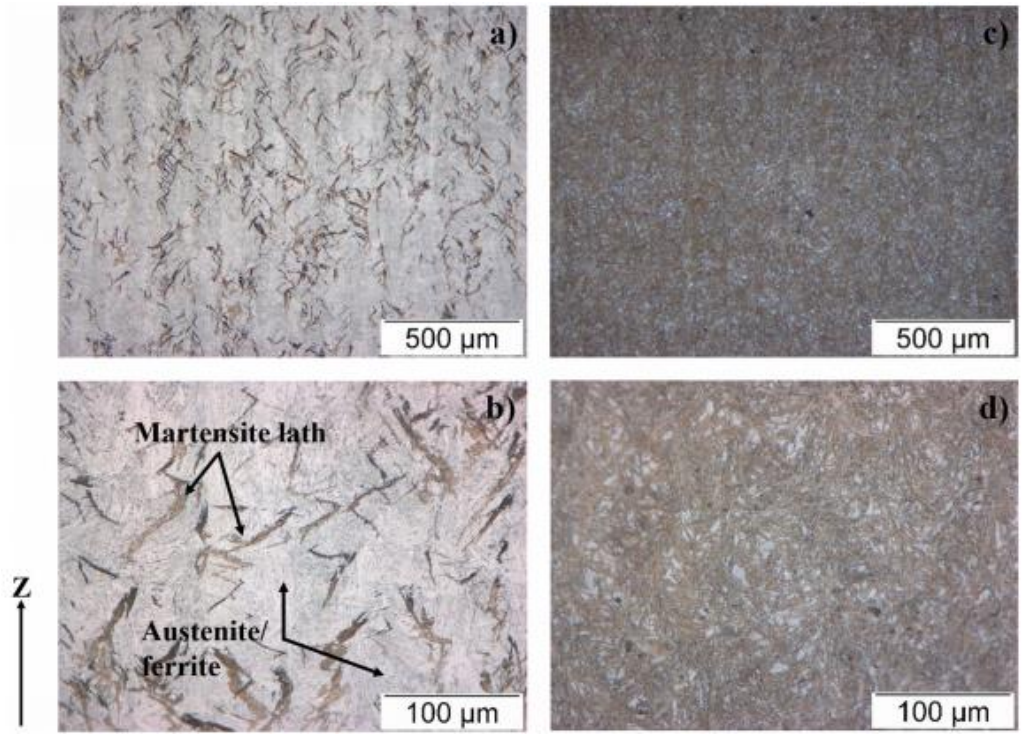

Figure 7. Optical microscopy of the manufactured specimens in their build direction, in as produced condition (a and b), and after heat treatment (c and d). (Nath et al. 2019)

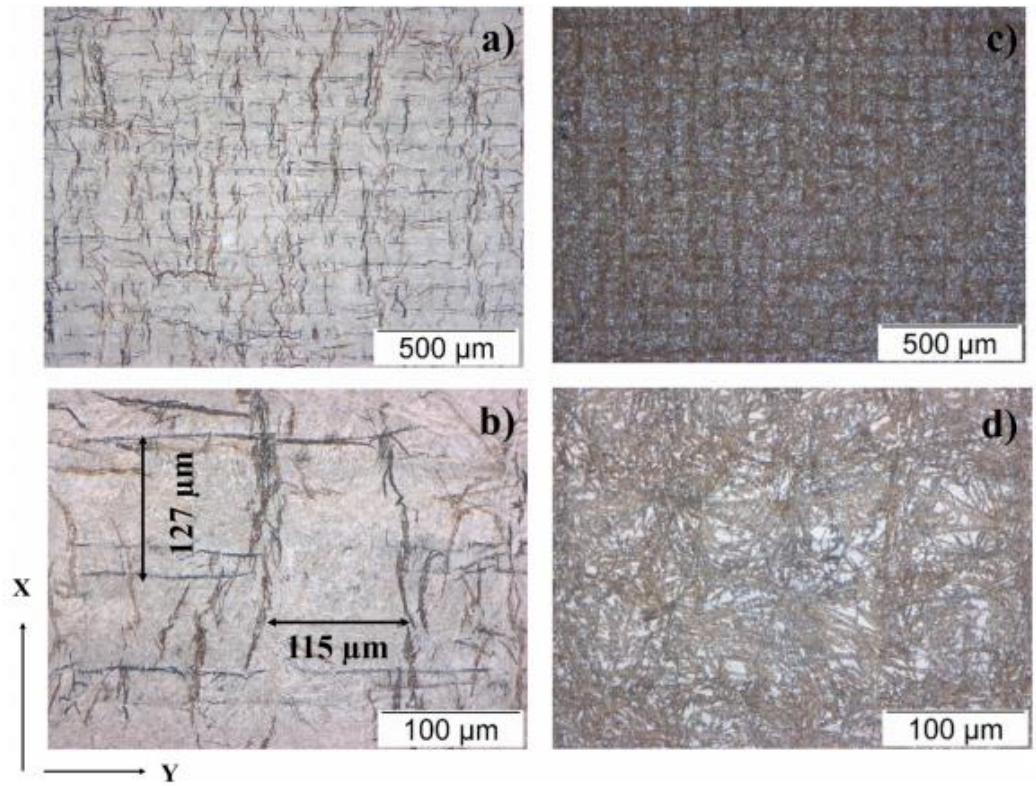

Figure 8. Optical microscopy of the scanned direction in as produced condition (a and b), and after heat treatment (c and d). (Nath et al. 2019)

In Figure 9 and Figure 10, the microstructure is shown in build direction of the as produced and heat treated parts, respectively. It can be seen that by increasing *t* the austenite content increases too, and with the *t* of 30 µm there are visible pores most likely due to lack-of-fusion. (Nath et al. 2020)

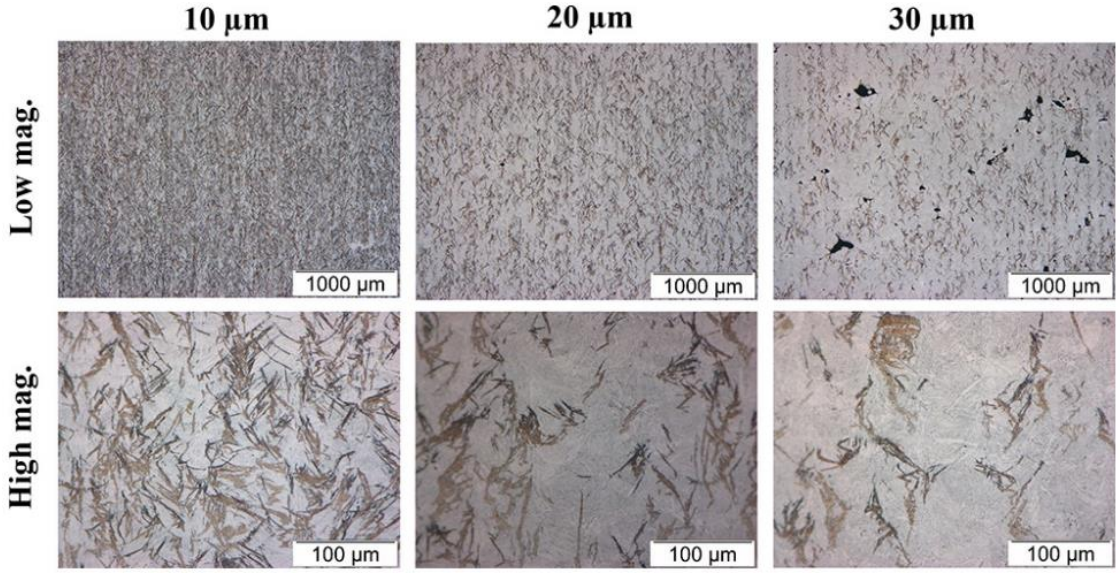

Figure 9. Microstructure of as produced parts in build direction using various layer thicknesses. (Nath et al. 2020)

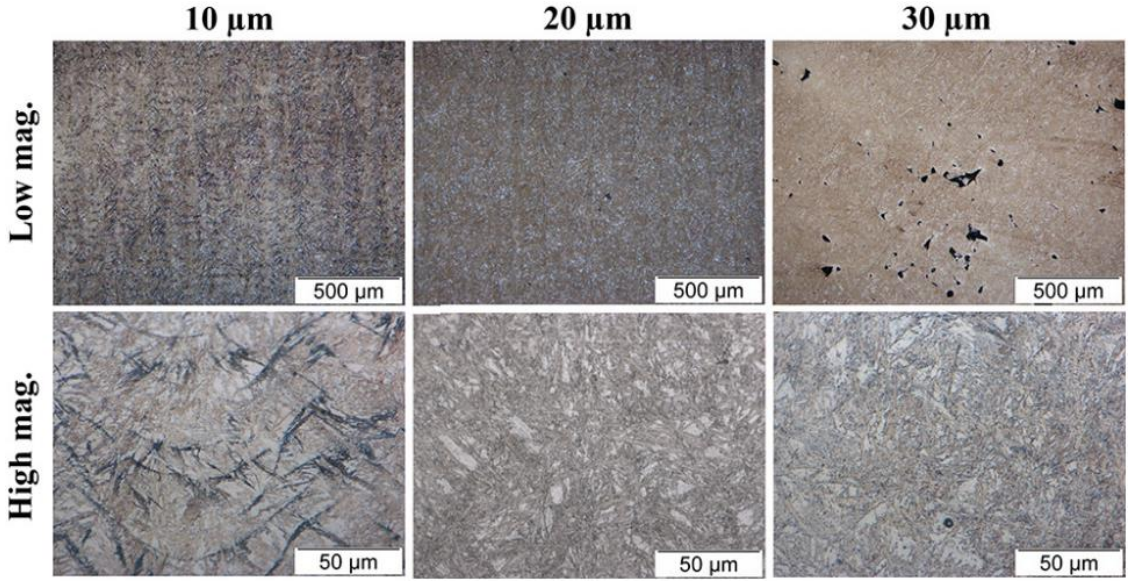

Figure 10. Microstructure of heat-treated parts in build direction using various layer thicknesses. (Nath et al. 2020)

5 DISCUSSION AND CONCLUSIONS

After reviewing the literature, the conclusion can be made that with L-PBF it is possible to produce 420 stainless steel parts with mechanical properties on par with, or even superior to conventionally manufactured wrought 420 stainless steel. Even when taking the highest R_m value listed for wrought 420, as shown in Table 2, being 1720 MPa, by the means of L-PBF there was a maximum reported R_m value of 1960 MPa by Tian et al. (2021). This section introduces the main findings regarding the effective parameters and their impact on the mechanical properties of produced 420 stainless steel. Moreover, the future studies due to the current gap of knowledge are presented.

5.1 Effects of parameters on L-PBF 420 stainless steel

The most important parameter for affecting the tensile properties of L-PBF 420 stainless steel is volumetric energy density E_v as it demonstrates the most observable trend. Increasing the E_v seems to increase the tensile strength of the produced 420 stainless steel too, as shown in Figure 3 and Figure 4. Also, a similar trend is observed in the rise of tensile strength after the produced material is heat treated. The reason is found in the increase of martensite content in the parts after heat treatment. Although E_v is the most important parameter it is still affected by the other parameters, thus they need to be in balance. A good example is given by the study of Shen et al. (2020) where the value of P was kept at the highest, while E_v was among the lowest. As a result, the tensile strength of the produced material was found to be among the lowest values. With improper parameter combination the mechanical properties might be lower than expected, and the parts might contain defects. In terms of tensile strength, the best parameter combination found in this thesis is P = 260 W, v = 1100 mm/s, h = 100 μm, and t = 30 μm (Tian et al. 2021).

As for the hardness evaluation, no considerable effect from E_v was reported. In almost all studies, the reported hardness values were at 50 HRC or above, which is comparable to wrought 420. Slight anomaly is the study by Shi et al. (2020) which reports hardness at the maximum of 37 HRC and Tian et al. (2021) did not measure the hardness.

There seems to be a threshold of 60 J/mm^3 for E_v to produce parts with a relative density of over 99 % when compared to wrought 420 stainless steel. The parts that were produced with a lower value of E_v than 60 J/mm^3 were the only ones to exhibit R_m values under 1000 MPa in the as produced state. Nath et al. (2020), reported porosities due to the lack-of-fusion in the microstructure of the produced material which may be the reason behind weaker mechanical properties. The sample size here is small and thus the parameter combination that produces parts with the best mechanical properties is not necessarily yet found.

5.2 Future studies

Based on the findings of the thesis, the following studies are suggested as future studies:

- One major finding which was noticed whilst searching the literature was the lack of data on the fatigue properties of 420 stainless steel produced with L-PBF. Hence, it is suggested to conduct fatigue testing on 420 stainless steel produced with L-PBF.
- Out of the articles only Nath et al. (2020) studied effect of a singular parameter, that being layer thickness *t*. In order to study the effect of *P*, *h*, and *v* separately, more testing is required where one parameter is varied while others are kept as a constant.
- Optimization of the process parameters for lower production times whilst maintaining the desirable properties.

6 SUMMARY

420 stainless steel is a martensitic stainless steel and thus has good tensile strength and corrosion resistance. R_m ranges from 650 to 1720 MPa, $R_{0,2}$ from 500 to 1480 MPa, and hardness of slightly above 50 HRC in hardened state. In this thesis the effect of manufacturing parameters on the mechanical properties of 420 stainless steel manufactured with L-PBF was studied. The work was carried out as a literature review, looking into the mechanical properties of 420 stainless steel manufactured with L-PBF. Wrought 420 was also discussed as a reference when studying the mechanical properties. The manufacturing parameters affecting the mechanical properties of L-PBF 420 stainless steel were discussed.

The manufacturing parameters were identified as laser power P, scanning speed v, hatch distance h, layer thickness t, and their combined effect as volumetric energy density E_v, which is commonly used in the literature. Typical defects that are caused by the parameters include keyhole porosity and lack-of-fusion porosity.

After reviewing available data in the literature on 420 stainless steel produced with L-PBF, it was found that with L-PBF it is possible to produce 420 stainless steel that has comparable mechanical properties to its wrought counterpart. Out of the discussed parameters, E_v was chosen as the most important one as it has a clear trend in its relation to the mechanical properties. As it has been demonstrated, i.e., by increasing E_v values, the tensile strength increases, too. E_v does not seems to affect the hardness of the material. Other parameters were also found to be important as they affect E_v meaning that they need to be well balanced to produce parts at desired quality.

LIST OF REFERENCES

Brnic, J., Turkalj, G., Canadija, M., Lanc, D., Krscanski, S. 2011. Martensitic stainless steel AISI 420—mechanical properties, creep and fracture toughness. Mechanics of time-dependent materials. Vol. 15. p. 341-352.

Coleman, A. J., Murray, K., Kearns, M., Tingskog, T. A., Sanford, B., Gonzalez, E. 2013. Properties of MIM AISI 420 via pre-alloyed and master alloy routes. 8 p.

Davis, J. R. 1998. Metals handbook. 2nd ed. ASM International. 1436 p.

Gibson I., Rosen, D., Stucker, B., Khorasani M. 2021 Additive Manufacturing Technologies. 3rd ed. Springer. Cham. 675 p.

Kumar, S., 2020. Additive Manufacturing Processes. Springer International Publishing. Cham. 205 p.

Nath, S. D., Gupta, G., Kearns, M., Gulsoy, O., Atre, S. V. 2020. Effects of layer thickness in laser-powder bed fusion of 420 stainless steel. Rapid prototyping journal. Vol. 26. p. 1197-1208.

Nath, S. D., Irrinki, H., Gupta, G., Kearns, M., Gulsoy, O., Atre, S. 2019. Microstructure-property relationships of 420 stainless steel fabricated by laser-powder bed fusion. Powder Technology. Vol. 343. p. 738-746.

Oliveira, J. P., LaLonde, A. D., Ma, J. 2020. Processing parameters in laser powder bed fusion metal additive manufacturing. Materials & Design. Vol. 193. 12 p.

Outokumpu Stainless, A. B. 2013. Handbook of stainless steel. Outokumpu Oyj. Espoo.

Saeidi, K., Zapata, D. L., Lofaj, F., Kvetkova, L., Olsen, J., Shen, Z., et al. 2019. Ultra-high strength martensitic 420 stainless steel with high ductility. Additive Manufacturing. Vol. 29. 6 p.

Saunders, M. 2017. X marks the spot - find ideal process parameters for your metal AM parts. [Accessed 1.4.2021] Available: https://www.linkedin.com/pulse/x-marks-spot-find-ideal-process-parameters-your-metal-marc-saunders

SFS-EN 10088-1. 2014. Stainless steels. Part 1: List of stainless steels. 68 p.

SFS-EN 10088-3. 2014. Stainless steels. Part 3: Technical delivery conditions for semi-finished products, bars, rods, wire, sections and bright products of corrosion resisting steels for general purposes. 76 p.

Shen, L. C., Yang, X. H., Ho, J. R., Tung, P. C., Lin, C. K. 2020. Effects of build direction on the mechanical properties of a martensitic stainless steel fabricated by selective laser melting. Materials. Vol. 13. 18 p.

Shi, Y., Xiong, X., Liu, Z., Yang, Y., Hou, J., Wu, S., et al. 2020. Mechanical Property Evaluation of a SLMed Martensitic Stainless Steel. Acta metallurgica sinica = 金属学报（英文版. Vol. 33. p. 1466-1476.

Thompson, S. 1999. Appendix V - Hardness conversion chart. Handbook of mold, tool and die repair welding. Woodhead Publishing p. 197-199.

Tian, Y., Chadha, K., Aranas, C. 2021. Laser powder bed fusion of ultra-high-strength 420 stainless steel: Microstructure characterization, texture evolution and mechanical properties. Materials Science and Engineering: A. Vol. 805.

Mechanical properties of L-PBF produced 420 stainless steel from the articles.

Article	Condition	Hardness	Yield strength, $R_{0,2}$ [MPa]	Ultimate tensile strength, R_m [MPa]	Elongation, ε [%]	Notes
(Nath et al. 2019)	As produced	55 HRC	700	1050	2.5	-
	Heat treated	53 HRC	950	1520	6.3	-
(Nath et al. 2020)	As produced	57 HRC	1020	1130	2.8	t = 10 μm
	Heat treated	55 HRC	1140	1540	6.2	t = 10 μm
	As produced	51 HRC	670	760	1.5	t = 30 μm
	Heat treated	49 HRC	865	1020	3.8	t = 30 μm
(Tian et al. 2021)	As produced	-	1080	1750	22.0	Transverse Toughness 11 J
	Heat treated	-	1380	1960	16.4	Transverse Toughness 35 J
	As produced	-	1057	1745	21.7	Build Toughness 12 J
	Heat treated	-	1355	1945	13.4	Build Toughness 31 J

Mechanical properties of L-PBF produced 420 stainless steel from the articles.

Article	Condition	Hardness	Yield strength, $R_{0,2}$ [MPa]	Ultimate tensile strength, R_m [MPa]	Elongation, ε [%]	Notes
(Saeidi et al. 2019)	As produced	650 HV 57 HRC	600	1670	3.5	-
	Heat treated	500 HV 49 HRC	1400	1800	25	-
(Shi et al. 2020)	As produced	310 HB 33 HRC	700	1050	1.25	Longitudinal
	Heat treated	326 HB 35 HRC	890	1050	11	
	As produced	350 HB 37 HRC	650	1300	6.25	Transverse
	Heat treated	326 HB 35 HRC	870	1000	11.5	
(Shen et al. 2020)	As produced	56 HRC	484	841	1.25	Thickness[1]
		53,1 HRC	506	873	1.26	Width[2]
		60,5 HRC	993	1495	1.68	Length[3]

[1] Build direction in along the thickness of test piece.
[2] Build direction in along the width of test piece.
[3] Build direction in along the lenght of test piece.

R_m and $R_{0,2}$ as functions of v.

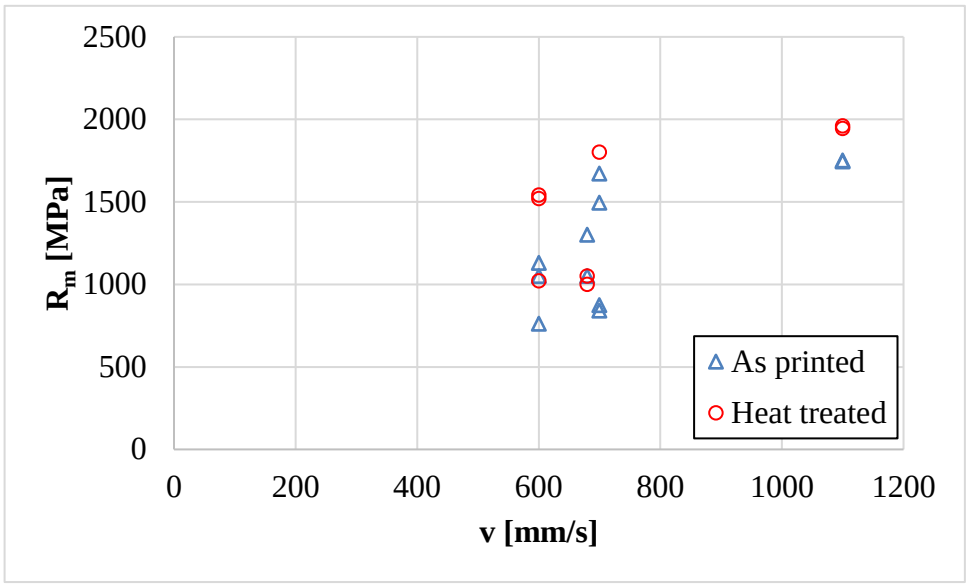

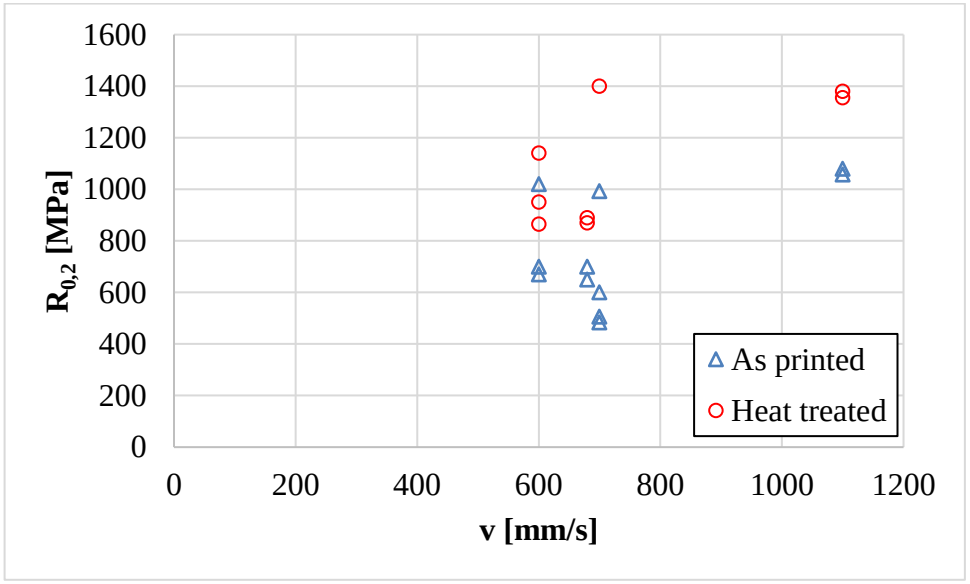

R_m and $R_{0,2}$ as functions of t.

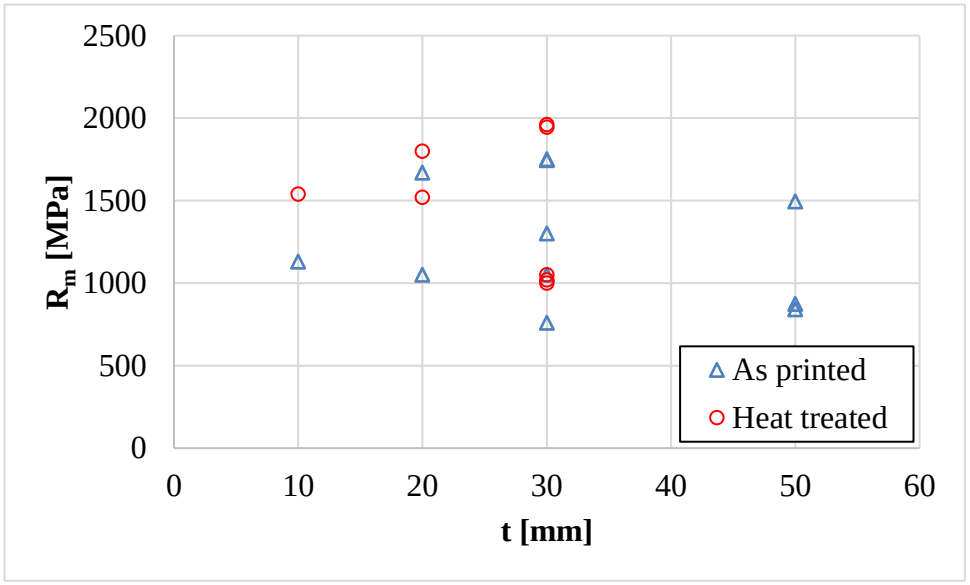

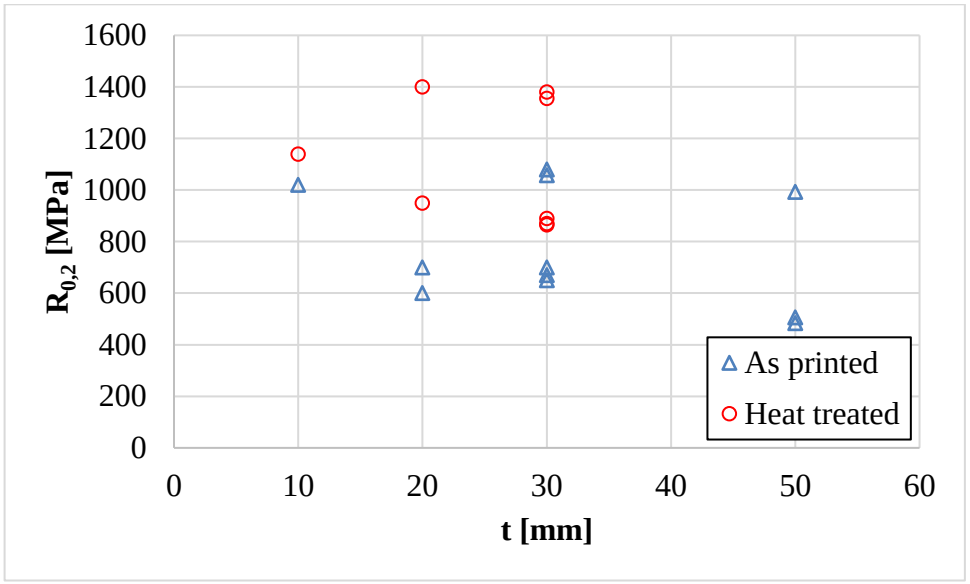

R_m and $R_{0,2}$ as functions of P.

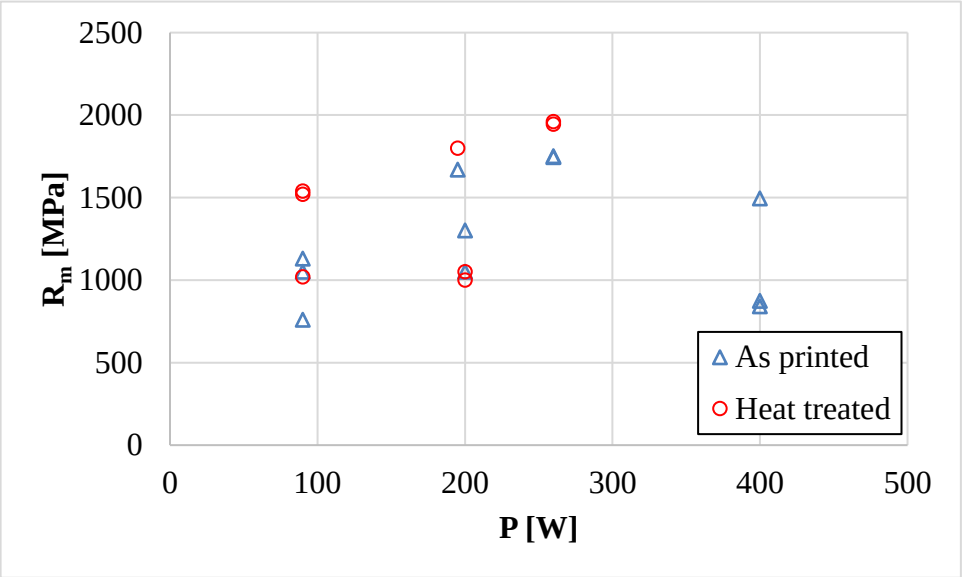

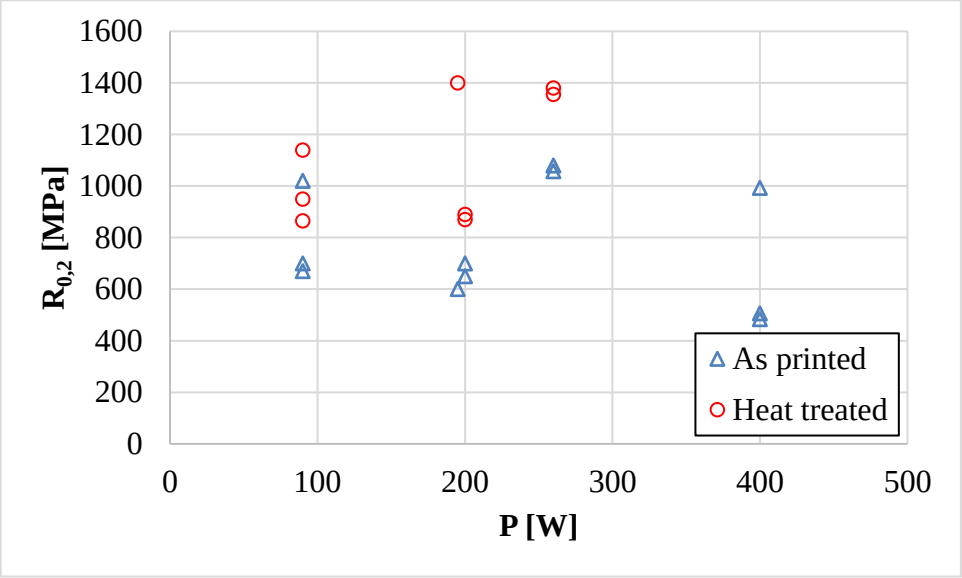

R_m and $R_{0,2}$ as functions of h.

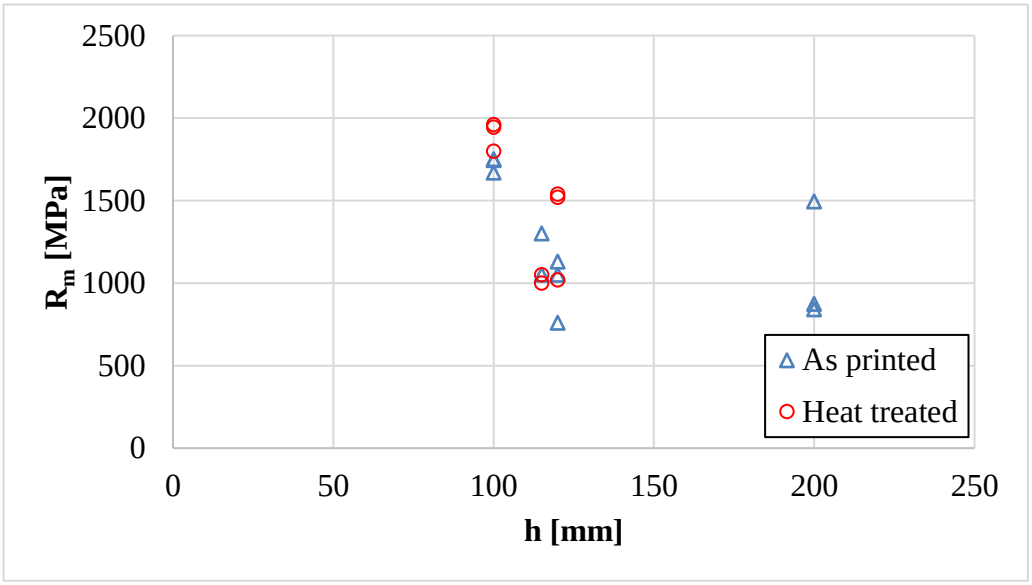

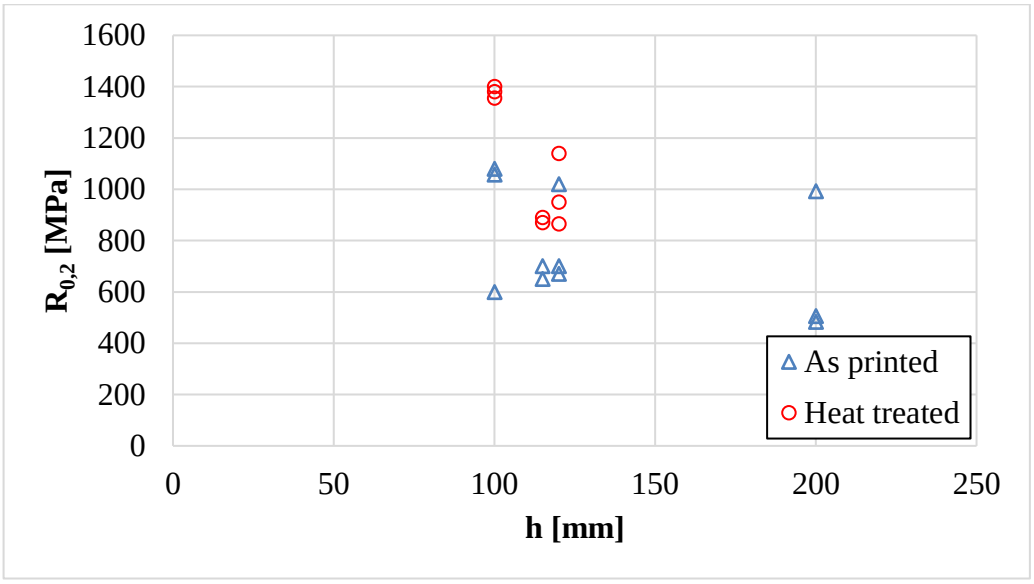

ε as a function of E_v.